Inorg. Chem. **2005**, *44*, 2358–2366

Structural, Magnetic, and Electrical Characterization of New Polycrystalline Phases of Nickel- and Platinum-Doped $[(DT\text{-}TTF)_n][Au(mnt)_2]$ ($n = 1, 2$)

Xavi Ribas,[†] Angelo Sironi,[‡] Norberto Masciocchi,*[,§] Elsa B. Lopes,[||] Manuel Almeida,[||] Jaume Veciana,[†] and Concepció Rovira*[,†]

Institut de Ciència de Materials de Barcelona, CSIC, Campus de la UAB, E-08193 Bellaterra, Spain, Dipartimento di Chimica Strutturale e Stereochimica Inorganica, Università di Milano and ISTM, via Venezian 21, 20133 Milano, Italy, Dipartimento di Scienze Chimiche ed Ambientali, Università dell'Insubria, via Valleggio 11, 22100 Como, Italy, and Departamento de Química, Instituto Tecnológico e Nuclear/CFMCUL, P-2686-953 Sacavém, Portugal

Received October 29, 2004

Doping of spin-ladder systems by isostructural paramagnetic complexes was attempted. Despite the close isostructural nature of the pure $(DT\text{-}TTF)_2[M(mnt)_2]$ (M = Au, Ni, Pt) end-members, which present a ladder structure, doping of the spin-ladder $(DT\text{-}TTF)_2[Au(mnt)_2]$ with either 5% or 25% $[M(mnt)_2]^-$ (M = Ni, Pt) generates two (metrically) *new* phases. Their markedly different crystal structures have been determined using laboratory X-ray powder diffraction data. $(DT\text{-}TTF)_2[Au_{0.75}Ni_{0.25}(mnt)_2]$ consists of a mixed-valence compound (of triclinic symmetry), which was only detected, pure or in a mixture of phases, when $[Ni(mnt)_2]^-$ was used as a dopant. Differently, the stoichiometric 1:1 $[DT\text{-}TTF][Au_{0.75}Pt_{0.25}(mnt)_2]$ monoclinic phase was found when $[Pt(mnt)_2]^-$ (in 5% and 25%) was employed as the doping agent. Remarkably, only in the 5% Pt doping experiment, the major component of the mixture was the ladder structure compound $(DT\text{-}TTF)_2[Au(mnt)_2]$ doped with minor amounts of Pt. This 5% Pt-doped specimen shows an EPR signal ($g = 2.0115$, $\Delta H_{pp} = 114$ G at 300 K) wider than the pure compound $(DT\text{-}TTF)_2[Au(mnt)_2]$, denoting exchange between the donor spins and $Pt(mnt)_2^-$ centers. The electrical transport properties of the 5% Pt-doped composition at high temperatures are comparable to those of $(DT\text{-}TTF)_2[Au(mnt)_2]$ with room-temperature conductivity $\sigma_{300K} = 13$ S/cm and thermopower $S_{300K} = 46$ μV/K, with a sharp transition at 223 K similar to that previously observed in the Cu analogue at 235 K.

Introduction

Spin-ladders are low-dimensional magnetic quantum systems that consist of a finite number of strongly magnetically coupled chains of spins that are the crossroads between one and two dimensions.[1−5] Among other features, the awkward dependence of the bulk magnetic properties with the even/odd number of legs in the ladder has attracted the interest of the scientific community. Indeed, it has been demonstrated that odd-leg ladders are gapless and behave as one-dimensional antiferromagnetic Heisenberg chains, whereas even-leg ladders exhibit a purely short-range spin correlation along the legs, consisting of spin pairs with a spin−spin correlation distance along the legs that show an exponential decay produced by the presence of a finite spin gap. Figure 1 exemplifies the magnetic nature of these extended systems.

One of the intriguing predictions for spin-ladder compounds is that light hole-doping can lead to superconductivity

* Authors to whom correspondence should be addressed. E-mail: cun@icmab.es (C.R.); norberto.masciocchi@uninsubria.it (N.M.).
[†] Institut de Ciència de Materials de Barcelona.
[‡] Università di Milano and ISTM.
[§] Università dell'Insubria.
[||] Instituto Tecnológico e Nuclear/CFMCUL.

(1) (a) Dagotto, E.; Rice, T. M. *Science* **1996**, *271*, 618−623. (b) Hiroi, Z.; Takano, M. *Nature* **1995**, *337*, 41−43.
(2) Dagotto, E.; Riera, J.; Scalapino, D. J. *Phys. Rev. B* **1992**, *45*, 5744.
(3) (a) Rice, T. M.; Goplan, S.; Sigrist, M. *Eurphys. Lett.* **1993**, *23*, 445. (b) Barnes, T.; Dagotto, E.; Riera, J. Swanson, E. S. *Phys. Rev. B* **1993**, *47*, 3196.
(4) (a) Troyer, M.; Tsunetsugu, H.; Würtz, D. *Phys. Rev. B* **1994**, *50*, 13515. (b) Troyer, M.; Zhitomirsky, M. E.; Ueda, K. *Phys. Rev. B* **1997**, *55*, 6117.
(5) Rovira, C. *Chem.—Eur. J.* **2000**, *6*, 1723−1729.

10.1021/ic048484d CCC: $30.25
Published on Web 02/18/2005

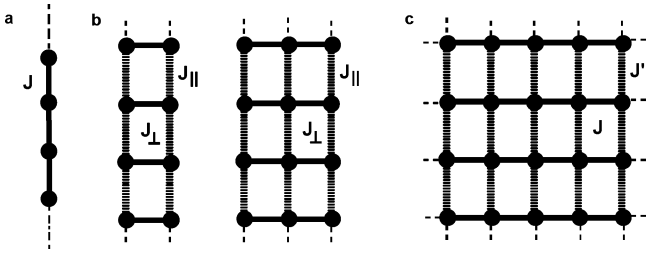

Figure 1. (a) Single one-dimensional chain ($n = 1$). (b) Ladders composed of two ($n = 2$) or three ($n = 3$) chains. (c) Two-dimensional square lattice which may be thought as an infinite array of coupled chains ($n \rightarrow \infty$).

on the basis that effective attraction between extra holes may arise from the magnetic interactions between the spins of the ladder.[1]

In our group we have characterized the molecular spin-ladder (DT-TTF)$_2$[Au(mnt)$_2$], $\mathbf{1}_{Au}$, consisting of a ladderlike structure with two interacting stacks of DT-TTF (dithiophene−tetrathiafulvalene) molecules building up the two-leg ladder, surrounded by stacks of closed-shell gold complex [Au(mnt)$_2$]$^-$ (mnt = maleonitriledithiolate) that magnetically isolate the ladders (see Figure 2).[6] In this ladder the (DT-TTF)$_2^{\bullet+}$ unit is the spin carrier and the magnetic behavior matches perfectly with that expected for a molecular spin-ladder.

The isostructural compounds where the gold complex has been changed by the corresponding monoanionic Ni or Pt complexes, (DT-TTF)$_2$[Ni(mnt)$_2$], $\mathbf{1}_{Ni}$, and (DT-TTF)$_2$[Pt(mnt)$_2$], $\mathbf{1}_{Pt}$, have also been characterized,[7] presenting an EPR signal with larger line width than the corresponding Au complex ($\mathbf{1}_{Au}$). The antiferromagnetic interaction of paramagnetic Ni^{III} and Pt^{III} centers with the organic spin carriers is clearly reflected in the susceptibility measurements, differing from the spin-ladder magnetic behavior.

In this paper we have explored the possibility of doping the spin-ladder (DT-TTF)$_2$[Au(mnt)$_2$] with different percentages of [Ni(mnt)$_2$]$^-$ and [Pt(mnt)$_2$]$^-$ to provoke a modification on the magnetic ladder to induce a magnetic defect that would interact with the spins of the ladder and to study how the magnetic properties are affected by the increasing concentration of extra paramagnetic centers. The original strategy for this work closely followed the alloying study of the two chain compounds (perylene)$_2$[M$_{1-x}$M′$_x$(mnt)$_2$] with M, M′ = Au, Pt, compounds which are isostructural to the DT-TTF analogues and where solid solutions could be obtained in an extended range of composition.[8] However, quite unexpectedly, the presence of these dopants in the DT-TTF compounds resulted in completely new structures (and stoichiometry), which were eventually determined by means of ab initio X-ray powder diffraction (XRPD) methods on very small quantities of polycrystalline materials. Only with low percentages (5%) of Pt(mnt)$_2$ as dopant, the ladder structure is maintained, its magnetic and electrical properties being described in the following.

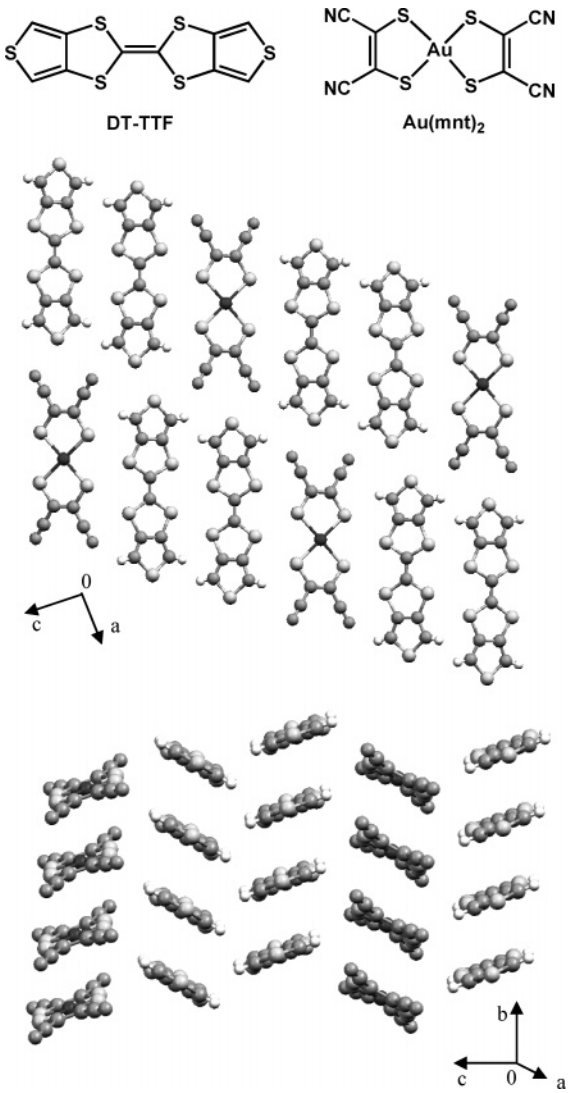

Figure 2. Schematic drawings of the top and side views of the crystal structure of the molecular spin-ladder (DT-TTF)$_2$[Au(mnt)$_2$] (atomic coordinates taken from ref 6).

Results and Discussion

Due to the synthetic difficulty to obtain a hole injection on the ladder chain, presumably leading to superconductivity as the theory predicts, we have investigated the electric and magnetic effects caused by doping the spin-ladder compound (DT-TTF)$_2$[Au(mnt)$_2$], $\mathbf{1}_{Au}$, with paramagnetic complexes. We have chosen the [Ni(mnt)$_2$]$^-$ and [Pt(mnt)$_2$]$^-$ complexes because $\mathbf{1}_{Ni}$ and $\mathbf{1}_{Pt}$ are known to be isostructural with the gold compound.[7] Therefore, we aimed at preparing doped systems maintaining (after doping) the same ladderlike crystal structure of their pure (Au, Ni, or Pt) end-members. We have performed two sets of doping experiments, with 5% and 25% content of [Ni(mnt)$_2$]$^-$ (or [Pt(mnt)$_2$]$^-$) complexes, with respect to the total [M(mnt)$_2$]$^-$ content.

In a standard preparation, we used a solution of the corresponding x% molar amount of (n-Bu$_4$N)[M(mnt)$_2$]$^-$ (M = Ni, Pt) with the (100 − x)% molar amount of (n-Bu$_4$N)-

(6) Rovira, C.; Veciana, J.; Ribera, E.; Tarrés, J.; Canadell, E.; Rousseau, R.; Mas, M.; Molins, E.; Almeida, M.; Henriques, R. T.; Morgado, J.; Schoeffel, J.-P.; Pouget, J.-P. *Angew. Chem., Int. Ed. Engl.* **1997**, *36*, 2324−2326.
(7) Ribera, E.; Rovira, C.; Veciana, J.; Tarrés, J.; Canadell, E.; Rousseau, R.; Molins, E.; Mas, M.; Schoeffel, J.-P.; Pouget, J.-P.; Henriques, R. T.; Morgado, J.; Almeida, M. *Chem.—Eur. J.* **1999**, *5*, 2025−2039.
(8) Matos, M. J.; Almeida, M.; Alcácer, L.; Henriques R. T. *Synth. Met.* **1997**, *86*, 2089.

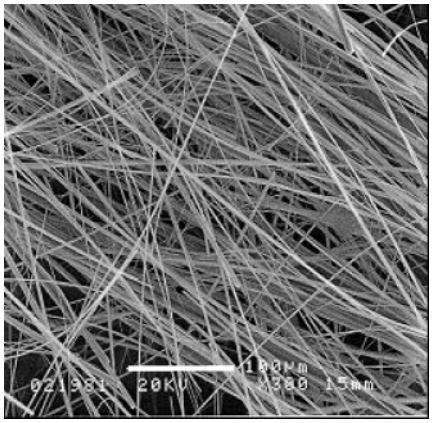

Figure 3. SEM image of crystals of **2**, containing a 25:75 Ni:Au molar ratio.

$[Au(mnt)_2]^-$ in CH_2Cl_2 as electrolyte in a standard electrocrystallization experiment with the donor DT-TTF. The products of all different experiments were analyzed by scanning electron microscopy (SEM), energy dispersive X-ray microanalysis (EDX), IR and UV−vis−NIR spectroscopy, electron paramagnetic resonance (EPR), and X-ray powder diffraction (XRPD).

For the sake of conciseness and clarity, the chemical formulas and the numbering scheme adopted in this paper are resumed as follows:

Isostructural *monoclinic* species **1**, $(DT\text{-}TTF)_2[Au(mnt)_2]$ ($\mathbf{1}_{Au}$), $(DT\text{-}TTF)_2[Ni(mnt)_2]$ ($\mathbf{1}_{Ni}$), $(DT\text{-}TTF)_2[Pt(mnt)_2]$ ($\mathbf{1}_{Pt}$), $(DT\text{-}TTF)_2[Cu(mnt)_2]$ ($\mathbf{1}_{Cu}$), $(DT\text{-}TTF)_2[Au_{0.95}Pt_{0.05}(mnt)_2]$ ($\mathbf{1}_{Au(Pt)}$).

Isostructural *triclinic* species **2**: $(DT\text{-}TTF)_2[Au_{0.75}Ni_{0.25}(mnt)_2]$ (**2**), $(DT\text{-}TTF)_2[Au_{0.95}Ni_{0.05}(mnt)_2]$ (**2′**). Isostructural *monoclinic* species **3**: $(DT\text{-}TTF)[Au_{0.75}Pt_{0.25}(mnt)_2]$ (**3**), $(DT\text{-}TTF)[Au_{0.95}Ni_{0.05}(mnt)_2]$ ($\mathbf{3}_{Ni}$).

Species of unknown structure: $(DT\text{-}TTF)_n[Au_{0.55}Pt_{0.45}(mnt)_2]_m$ (**3′**).

Doping with 25% $[Ni(mnt)_2]^-$. The crystalline material obtained by using a 1:3 $[Ni(mnt)_2]^-/[Au(mnt)_2]^-$ molar amounts in the electrocrystallization experiment was initially studied by scanning electronic microscopy. SEM images indicated the formation of very thin needles (ca. 1 μm wide and up to 1 mm long; see Figure 3). EDX confirmed (within the experimental error) the expected 1:3 molar ratio of the Ni:Au elements in all different sections of the crystals, indicating a homogeneous distribution of the doping agent. This observation suggested that such needles were likely of single-crystal nature, but they were definitely too small to be of any use for conventional single-crystal diffraction analyses. Thus, we resorted to ab initio XRPD methods to gather structural information from this sample, which eventually led to the model presented hereafter as **2**.

Crystals of **2**, with $(DT\text{-}TTF)_2[Au_{0.75}Ni_{0.25}(mnt)_2]$ formulation, are triclinic (see Experimental Section for details) and are based on segregated stacks of donor and acceptor units along the *b* axis (approximately 3.8 Å). The unit cell contains two distinct organic cations and one metal complex, all lying onto crystallographic inversion centers. Figure 4 shows a drawing of the crystal structure viewed approximately down

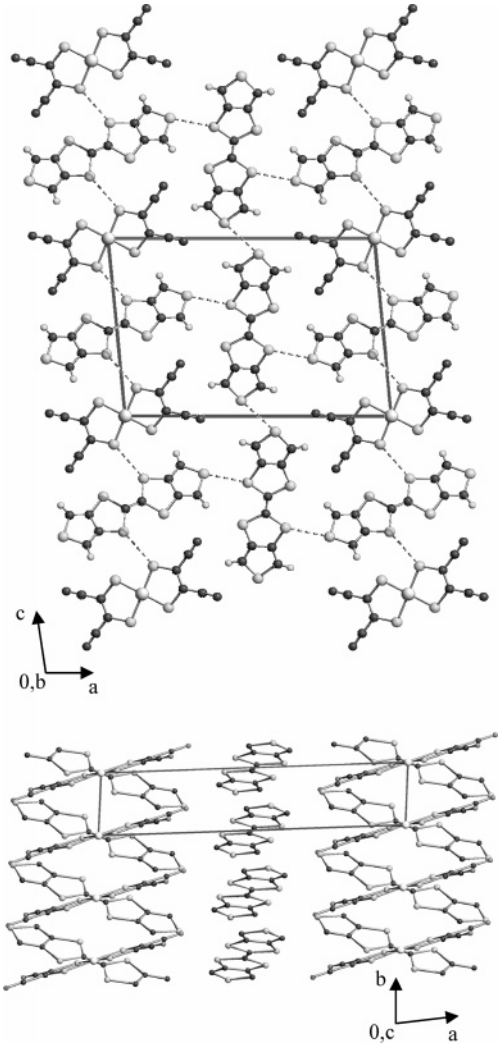

Figure 4. Top: Drawing of the crystal structure of the $(DT\text{-}TTF)_2[Au_{0.75}Ni_{0.25}(mnt)_2]$, **2**, down the shortest axis *b*, showing the shortest S···S contacts (<3.6 Å) as fragmented lines. Bottom: Packing motif viewed down *c* (hydrogen atoms omitted for clarity).

[010], where the relative orientations of the different molecules can be easily appreciated.

Each stack of $M(mnt)_2$ anions is completely surrounded by stacks of the donors preventing any contact with other metal complex chains. In the *ac* plane, the metal complexes interact, through a number of S···S short nonbonded contacts (fragmented lines in Figure 4), to only *one* of the DT-TTF molecules (S···S values lying in the 3.40−3.77 Å range) lying almost parallel to the complex; the resulting ribbons, with $(DT\text{-}TTF)[Au_{0.75}Ni_{0.25}(mnt)_2]$ formulation (and running along *c*), share further contacts with the other DT-TTF groups (S···S = 3.26 Å), which present a rather different orientation (nearly vertical in Figure 4). The *inter*molecular S···S contact between two DT-TTF in different type of chains are rather short, but not unusual, since interactions of the order of 3.30 Å (or even below) are known for quasi-dimeric moieties of this kind.[9] Thus, roughly speaking, crystals of **2** (of overall A_2B stoichiometry) contain $[Au_{0.75}Ni_{0.25}(mnt)_2]^-$ anions embedded in an extended framework of heavily linked DT-TTF molecules.

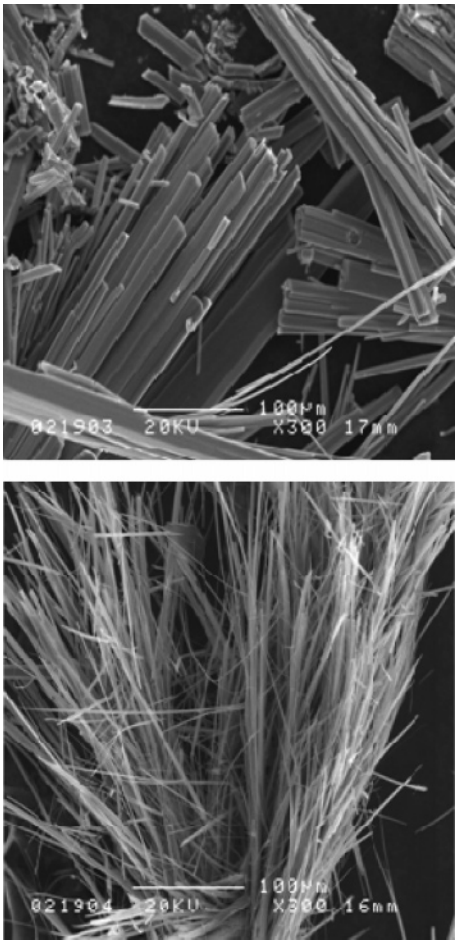

Figure 5. SEM images of crystals of compound **3** (containing a 1:3 Pt:Au molar ratio; top) and of the contaminating minor phase, **3′** (containing 1:1 Pt:Au molar ratio; bottom).

In terms of oxidation state of the molecules, a charge transfer band A is clearly observed in the NIR spectrum of the sample in KBr pellet, which indicates the presence of a mixed-valence compound, in accordance with the obtained formulation. Often, the C═C bond distances observed in the DT-TTF molecules have been correlated with the effective charge on these organic fragments (in our case, 1/2+). However, the required accuracy falls well beyond the possibilities of XRPD, *even when extremely highly polycrystalline materials are available*.[10]

Doping with 25% [Pt(mnt)$_2$]$^-$. The crystalline material obtained by using a 1:3 [Pt(mnt)$_2$]$^-$:[Au(mnt)$_2$]$^-$ molar ratio in the electrocrystallization experiment was also analyzed by scanning electron microscopy. SEM images indicated the formation of crystals with two different morphologies: the most abundant material consists of block-shaped crystals of typical $5 \times 10 \times 200$ μm size (see Figure 5, top) that, within the experimental error, contained a 1:3 Pt:Au molar ratio in all different sections of the crystals, indicating a homogeneous distribution of the doping agent. A small percentage of a crystal phase with different morphology (much thinner hairylike crystals, as in Figure 5, bottom) was detected and studied by EDX, which indicated a 1:1 *homogeneous* Pt:Au molar ratio. As anticipated for **2**, also in this case the major component of the mixture was fully characterized by ab initio XRPD and will hereafter labeled as **3**. In contrast, the paucity of the contaminant crystals, **3′**, did not allow any quantitative structural study; indeed, their XRPD data showed a complex trace in which peaks of species **3** were emerging from a heavily structured background, together with a number of ancillary (weaker) reflections *not* belonging to any known crystal phase in the DT-TTF/M(mnt)$_2$ family (M = Au, Pt, Ni). Thus, among the many (DT-TTF)$_n$[M(mnt)$_2$] systems (n = 1, 2), this new species, of yet unknown formulation, awaits a more selective preparation and a complete structural characterization.

Crystals of **3**, which possess the *unexpected* (DT-TTF)[Au$_{0.75}$Pt$_{0.25}$(mnt)$_2$] formulation (1:1 donor:acceptor stoichiometry), not found before for the samples with nonmixed metals, are monoclinic and are based upon a short segregated stacking (determined by the length of the *c* axis, ca. 3.8 Å) of these two moieties, the organic cation and the metal complex, both lying onto distinct crystallographic inversion centers. Figure 6 shows a drawing of the crystal structure viewed along the *c* axis, where the relative orientations of the different molecules can be easily appreciated. The donor and acceptor stacks alternate along the *a* and *b* axes. In the *ab* plane, the differently charged ions pack in a *centered* rectangular lattice, with formal (4,4) coordination; the presence of direct parallel stacking of all molecules along the short *c* axis, which disrupts an easily foreseeable three-dimensional (6,6) packing (of the NaCl type) for the present formal AB stoichiometry, must therefore be a manifestation of a significant interaction between the DT-TTF cations, which stabilize the overall crystal structure through the formation of infinite (DT-TTF)$_n$ chains running in the [001] direction. Significant nonionic interactions occur also between the metal complexes and the DT-TTF cations, short S···S intermolecular distances (<3.6 Å) being observed. Moreover, on the basis of the presently available XRPD data, we cannot state whether *c* is *exactly* normal to the *ab* plane, but even if slight deviations are present, they would not significantly change the crystal packing pattern.[11]

Doping with 5% [Ni(mnt)$_2$]$^-$. The analysis of the SEM images of the crystalline material obtained by using a 5% molar amount of [Ni(mnt)$_2$]$^-$ related to the molar amount of [Au(mnt)$_2$]$^-$ in the electrocrystallization experiment indicated the formation of a unique morphology, that of very thin hairylike dark crystals (see Figure 7). In all of them the

(9) Imai, H.; Otsuka, T.; Naito, T.; Awaga, K.; Inabe, T. *J. Am. Chem. Soc.* **1999**, *121*, 8098. Devic, T.; Domercq, B.; Auban-Senzier, P.; Molinié, P.; Fourmigué, M. *Eur. J. Inorg. Chem.* **2002**, 2844. Akutsu, H.; Akutsu-Sato, A.; Turner, S. S.; Day, P.; Canadell, E.; Firth, S.; Clark, R. J. H.; Yamada, J.; Nakatsuji, S. *Chem. Commun.* **2004**, 18.

(10) The use of rigid bodies from previously determined (single-crystal) structures, as extensively described in the Experimental Section, only allows the detection of the overall stoichiometry and, of higher importance, of the crystallochemical packing features responsible for the magnetic and conducting behaviors described below.

(11) While we were writing this paper, the single-crystal X-ray analysis (Ribas, X.; Mas-Torrent, M.; Pérez-Benítez, A.; Dias, J. C.; Alves, H.; Lopes, E. B.; Henriques, R. T.; Molins, E.; Santos, I. C.; Wurst, K.; Faury-Leylekian, P.; Almeida, M.; Veciana, J.; Rovira, C. *Adv. Funct. Mater.*, in press) of the (DT-TTF)[Cu(mnt)$_2$] salt showed a crystal structure closely related to that of **3**, thus confirming the value of our XRPD analysis.

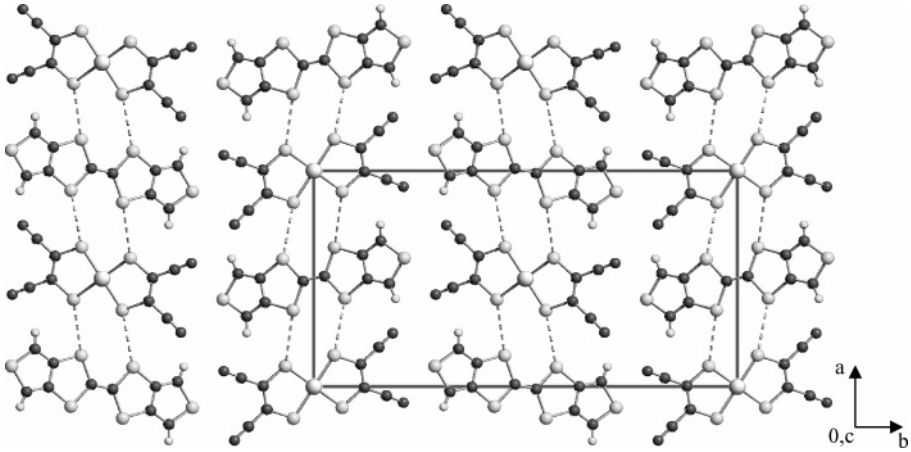

Figure 6. Drawing of the crystal structure of the (DT-TTF)[$Au_{0.75}Pt_{0.25}(mnt)_2$], **3**, down the shortest axis *c*, showing the short S···S contacts (<3.6 Å) as fragmented lines.

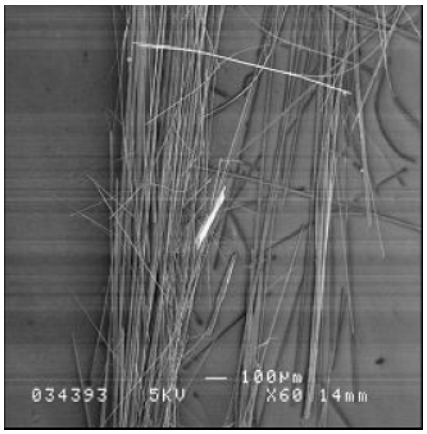

Figure 7. SEM image of the material formed by 5% Ni doping. Despite the observation of a unique morphology, this polycrystalline material is a mixture of **2′** and $\mathbf{3}_{Ni}$ crystals in a 32% and 68% ratio, respectively (as deduced from quantitative Rietveld XRPD analysis).

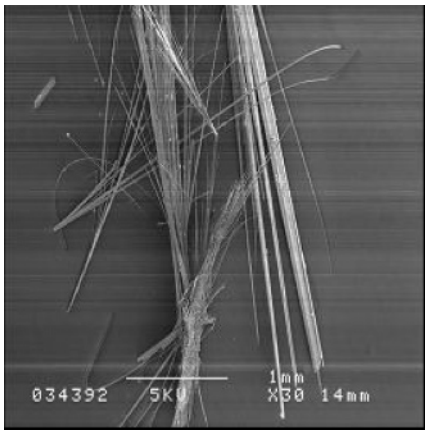

Figure 8. SEM image of the material formed by 5% Pt doping. This polycrystalline material is a mixture of "spin-ladder phase" crystals $\mathbf{1}_{Au(Pt)}$ and the (DT-TTF)[(Au,Pt)$(mnt)_2$] (**3′**) phase in a 85% and 15% ratio, respectively (as deduced from quantitative Rietveld XRPD analysis).

Ni content was in the lower limit of detection by EDX microanalysis, and what was possible to infer from the data was that the Ni content, if any, was less than the 5% molar in relation to total metal. This sample gave a rich XRPD pattern, which could be easily interpreted on the basis of the known structures of the crystals of **2** and **3**: quantitative analysis performed by the Rietveld method allowed one to detect the relative proportions, i.e. 32% vs 68%, for (DT-TTF)$_2$[(Au,Ni)$(mnt)_2$], **2′**, and (DT-TTF)[(Au,Ni)$(mnt)_2$], $\mathbf{3}_{Ni}$, respectively.

Doping with 5% $[Pt(mnt)_2]^-$. The crystalline material obtained by using a 5% molar amount of $[Pt(mnt)_2]^-$ showed a unique morphology, that of long thin and dark-green plate-shaped crystals (see SEM image in Figure 8). As in the previous experiment with 5% $[Ni(mnt)_2]^-$, the EDX data indicated less than the 5% molar of Pt in relation to total metal. Also this sample gave a rich XRPD pattern, which could be easily interpreted on the basis of the known structures of (DT-TTF)$_2$[$Au(mnt)_2$], $\mathbf{1}_{Au}$, and **3** crystals: quantitative analysis performed by the Rietveld method allowed one to detect their relative proportions, i.e. 85% vs 15%, for (DT-TTF)$_2$[(Au,Pt)$(mnt)_2$], $\mathbf{1}_{Au(Pt)}$, and (DT-TTF)-[(Au,Pt)$(mnt)_2$], **3′**, respectively. Note that the triclinic species **2** was not formed when platinum was used as a dopant, while it was persistently observed when Ni(III) ions were present.

EPR Studies. The magnetic behavior of species **2**, **3**, and $\mathbf{1}_{Au(Pt)}$ was studied by EPR on polycrystalline (**2**, **3**) or single-crystal ($\mathbf{1}_{Au(Pt)}$) samples from room temperature down to 110 K.

The EPR spectra of the new crystal phase (DT-TTF)$_2$-[$Au_{0.75}Ni_{0.25}(mnt)_2$] (**2**) shows at room temperature a single line centered at $g = 2.0107$, with a line width value of $\Delta H_{pp} = 43$ G. Upon cooling of the sample below 200 K, this line gradually resolves into three lines typical for a system with rhombic *g* anisotropy, with values at the lowest temperature measured (112 K) of $g_1 = 2.034$, $g_2 = 2.0138$, and $g_3 = 1.998$. This behavior has been compared with the EPR signal evolution while decreasing the temperature for the (*n*-Bu_4N)-[$Ni(mnt)_2$] salt,[12] where the *g* anisotropy is only seen below 100 K ($g_1 = 2.150$, $g_2 = 2.045$, and $g_3 = 1.992$ at 77 K). From this we can conclude that the EPR behavior for compound **2** results from the interaction of the organic radical and the paramagnetic metal subsystems in all the temperature

(12) The EPR parameters at 300 K for the (*n*-Bu_4N)[$Ni(mnt)_2$] salt are $g \sim 2.050$ and $\Delta H_{pp} > 2000$ G, and those for the (*n*-Bu_4N)[$Pt(mnt)_2$] salt are $g \sim 2.070$ and $\Delta H_{pp} > 2000$ G.

range measured. Specifically, at low temperature the g anisotropy of the $[Ni(mnt)_2]^-$ is clearly affected by the presence of the DT-TTF radicals.

Compound [DT-TTF][$Au_{0.75}Pt_{0.25}$(mnt)$_2$] (**3**), with a 1:1 stoichiometry, shows an EPR behavior similar to that of **2**, with a single wide EPR signal at room temperature (g = 2.0157, ΔH_{pp} = 200 G), which gradually also resolves below 200 K into three signals characteristic of rhombic g anisotropy (g_1 = 2.244, g_2 = 2.053, and g_3 = 1.822 at 122 K). The comparison with the EPR behavior of the salt (n-Bu_4N)[Pt(mnt)$_2$],[12,13] where the g anisotropy is again observed below 100 K (g_1 = 2.229, g_2 = 2.070, and g_3 = 1.834 at 77 K), points toward the interaction between the two paramagnetic subsystems in **3** but, however, of a lower magnitude than in the Ni case, since the g values at low temperatures are similar.

Finally, the EPR study of one oriented single crystal of the doped ladder structure [(DT-TTF)$_2$][(Au,Pt)(mnt)$_2$] (**1**$_{Au(Pt)}$), with a Pt content less than 5%, clearly confirms the presence of paramagnetic $Pt(mnt)_2^-$ anions in the structure. Thus, at room temperature both the g values and, especially, the line width parameters in two different orthogonal orientations of the crystal ($H \parallel a^*$, g = 2.0152, ΔH_{pp} = 132 G; $H \parallel c^*$, g = 2.0115, ΔH_{pp} = 114 G) are different from those of the pure gold spin-ladder system ($H \parallel a^*$, g = 2.0131, ΔH_{pp} = 43 G; $H \parallel c^*$, g = 2.0052, ΔH_{pp} = 26 G),[6] which clearly demonstrates the suspected presence of paramagnetic Pt(mnt)$_2$. The temperature dependence of the EPR signal intensity from room temperature down to 120 K shows a gradual increase until 140 K, and stabilization below this temperature. At the lowest temperature measured (124 K) the single signal is found centered at the same g value but narrowed to ΔH_{pp} = 86 G, indicating a strong interaction between the organic radicals and the paramagnetic anions.

Electrical Transport Measurements. In regard to the conductivity measurements, only compound (DT-TTF)$_2$[($Au_{0.95}Pt_{0.05}$)(mnt)$_2$] (**1**$_{Au(Pt)}$) has the proper structure to deserve a complete study of the transport properties. The electrical conductivity (σ) measurements of the ladder structure **1**$_{Au(Pt)}$ show a room-temperature conductivity of σ_{300K} = 13 S/cm, only slightly larger than that of the pure gold compound (8 S/cm)[6,7] following a semiconducting regime with an activation energy of 0.074 eV (see Figure 9). However, at variance with the pure Au analogue where this activation only presents a broad maximum centered around 220 K as shown also in Figure 9,[6] in crystals of this solid solution we observe at 223 K a very sharp maximum of the activation energy, clearly denoting a second-order transition.

Thermopower measurements (S) confirm the occurrence of this transition (Figure 9). At room temperature thermopower is 46 μV/K and decreases smoothly upon cooling, again in a fashion comparable to that of (DT-TTF)$_2$[Au(mnt)$_2$] (**1**$_{Au}$) until 223 K. Below this temperature it deviates from the behavior of **1**$_{Au}$, decreasing fast and becoming negative, following a typical semiconducting regime.

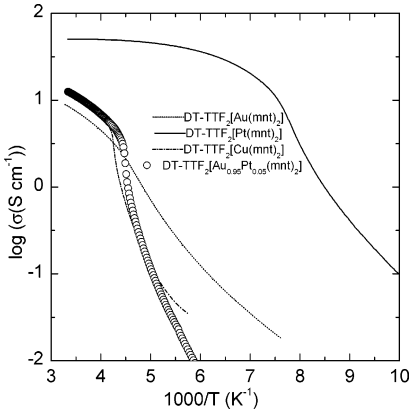

Figure 9. Plot of the electrical conductivity (σ) as a function of the inverse of the temperature (T) of the doped compound [(DT-TTF)$_2$][(Au,Pt)(mnt)$_2$] (**1**$_{Au(Pt)}$) (open circles) and the isostructural ladder compounds **1**$_{Au}$ (dotted line),[6] **1**$_{Pt}$ (solid line),[7] and **1**$_{Cu}$ (dashed line).[14]

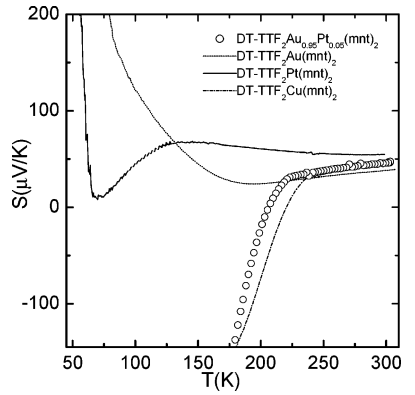

Figure 10. Plot of the absolute thermopower (S) versus the temperature (T) of the doped compound [(DT-TTF)$_2$][(Au,Pt)(mnt)$_2$] (**1**$_{Au(Pt)}$) (open circles) and the isostructural ladder compounds **1**$_{Au}$ (dotted line),[6] **1**$_{Pt}$ (solid line),[7] and **1**$_{Cu}$ (dashed line).[14]

This behavior of the solid solution with a transition at 223 K is very similar to that previously reported in the Cu analogue, (DT-TTF)$_2$[Cu(mnt)$_2$] (**1**$_{Cu}$), also depicted in Figures 9 and 10 ($\sigma_{RT} \sim$ 12 S/cm, and S_{RT} = 45 μV/K), where the second-order transition occurs at 235 K.[11,14] The diffuse X-rays scattering studies in the Cu compound show that this transition is due to a dimerization of the unit cell, ascribed to the donor stacks.[11,14] This dimerization presents long-range order at variance with the Au compound where the coherence length of the dimerization was of the order of only ~60 Å (~15 unit cells).

Therefore, we believe that the transition observed in this 5% Pt-doped composition is also due to this dimerization, being sharp due to the better sample quality (which allows the establishment of a tridimensional long-range order) rather than to any doping effect that, in this case, besides the magnetic properties, should not affect the conduction taking place in the donor stacks.

Conclusions

In this work, doping of spin-ladder systems by isostructural paramagnetic complexes has been attempted. Surprisingly,

(13) Kirmse, R.; Dietzsch, W.; Solov'ev, B. V. *J. Inorg. Nucl. Chem.* **1977**, *39*, 1157.

(14) Dias, J. C.; Lopes, E. B.; Santos, I. C.; Duarte, M. T.; Henriques, R. T.; Almeida, M.; Ribas, X.; Rovira, C.; Veciana, J.; Foury-Leylekian, P.; Pouget, J.-P.; Auban-Senzier, P.; Jérome, D. *J. Phys. IV* **2004**, *114*, 497−499.

Table 1. Synoptic Collection of Crystal Data for the Two Structurally Characterized Species

param	(DT-TTF)$_2$[Au$_{0.75}$Ni$_{0.25}$(mnt)$_2$]	(DT-TTF)[Au$_{0.75}$Pt$_{0.25}$(mnt)$_2$]
labeling	**2**	**3**
formula	$C_{28}H_8Au_{0.75}S_{16}N_4Ni_{0.25}$	$C_{18}H_4Au_{0.75}S_{10}N_4Pt_{0.25}$
fw	1075.85	793.41
cryst system	triclinic	monoclinic
space group	$P\bar{1}$	$P2_1/a$[a]
a, Å	18.554(3)	12.321(1)
b, Å	3.8188(4)	24.121(1)
c, Å	12.555(2)	3.80[a]
α, deg	97.17(1)	90[a]
β, deg	85.09(1)	90[a]
γ, deg	86.41(1)	90
V, Å^3	876.9(2)	1129[a]
Z	1	2
D_{calc}, g cm^{-3}	2.034	2.333[a]
method	powder XRD	powder XRD
2θ range, deg	4−64	7−64
N_{data}	3001	2851
R_p	0.069	0.096
R_{wp}	0.094	0.129
R_{Bragg}	0.046	0.050

[a] See the Experimental Section for the significance of these data.

despite the very close isostructural nature of the pure (DT-TTF)$_2$[M(mnt)$_2$] (M = Au, Ni, Pt) end-members, which present a ladderlike structure of donors, doping of the spin-ladder compound (DT-TTF)$_2$[Au(mnt)$_2$] with either a 5% or 25% molar amount of [M(mnt)$_2$] (M = Ni, Pt) (with respect to the total [M(mnt)$_2$]) does not lead preferentially to the formation of the ladder structure but generates two new phases with markedly different structures and new molecular packing patterns. Species **2** consists of a mixed-valence compound with a A_2B stoichiometry, which was only detected, pure or in a mixture of phases, when [Ni(mnt)$_2$]$^-$ (either 5% or 25%) was used as a dopant. Differently, the phase **3** with an AB stoichiometry was found when [Pt(mnt)$_2$]$^-$ (in 5% and 25%) was employed as the doping agent, as well as when [Ni(mnt)$_2$]$^-$ was added in smaller quantities (5%).

Noteworthy, only in the case of 5% doping with [Pt(mnt)$_2$]$^-$, the most abundant phase is the ladderlike structure. Careful refinement of the lattice parameters of this phase suggests a *very strong similarity* (but *not* identity, in the statistical sense) with those of pristine (DT-TTF)$_2$[Au(mnt)$_2$], suggesting possible partial inclusion of platinum ions. EPR characterization clearly confirms the partial inclusion of paramagnetic Pt ions in the ladder structure. The electrical conductivity behavior of the semiconducting Pt-doped ladder (**1**$_{Au(Pt)}$) structure (σ_{RT} = 13 S/cm) is similar to that reported for the pure gold spin-ladder and indeed parallels that of the copper spin-ladder, with a sharp transition at 223 K. These results are therefore the evidence of the first synthesis of a magnetically doped spin-ladder compound. However, they contrast with the (perylene)$_2$[Au$_{1-x}$Pt$_x$(mnt)$_2$] system, where solid solutions could be obtained in the more extended range $0 < x \leq 0.40$ and $x \geq 0.98$.[8,15] The main structural details and physical properties of all compounds are summarized in Table 2.

(15) Matos, M. J. Ph.D. Thesis, Technical University of Lisbon, 2001.

The presence of minor amounts of paramagnetic dopant seems to be insufficient to induce any significant effect in the conducting DT-TTF subsystem. On the contrary, attempts to increase the dopant content have led to new crystal phases and, in many cases, to mixtures of them. The latter complicates enormously the study of these systems, but nevertheless, further experiments on the magnetic influence of the dopant, such as magnetic susceptibility measurements down to liquid-He temperature, are in progress.

Experimental Section

Preparation of Samples. (DT-TTF)$_2$[Au/Ni(mnt)$_2$] (95:5 Au/Ni). A 0.238 mg (4.1×10^{-4} mmol) amount of (n-Bu$_4$N)[Ni(mnt)$_2$] and 5.48 mg (7.6×10^{-3} mmol) of (n-Bu$_4$N)[Au(mnt)$_2$] were dissolved in 12 mL of CH_2Cl_2 (Aldrich, HPLC grade). This solution was split in two: One portion (6 mL) was used to further dissolve 2.54 mg (8.03×10^{-3} mmol) of the donor DT-TTF, later placed in the anodic side of an H-shaped cell. The cathodic side of the cell was filled with the other aliquot (6 mL) of the doped acceptor solution. The molar ratio between the different species in solution was 1:0.95:0.05 (DT-TTF:Au(mnt)$_2$:Ni(mnt)$_2$). Then, the electrocrystallization experiment was started by applying a 1 μA constant current through two platinum electrodes (~0.5 cm^2 surface area) immersed in each side of the cell during 6 days, causing the growth of black thin crystals on the anodic electrode. The crystals were collected and washed with diethyl ether.

The compounds with the other doping combinations (95:5 Au/Pt; 75:25 Au/Ni; 75:25 Au/Pt) were synthesized in a similar manner, using 2.5 mg of the DT-TTF donor and the corresponding amount of transition metal complexes to keep the molar ratios as indicated.

[(DT-TTF)$_2$][Au$_{0.75}$Ni$_{0.25}$(mnt)$_2$] (2). IR (KBr pellet; cm^{-1}): ν = 3102, 1507, 1345, 1231, 1146, 840, 766, 705, 420 ("A" band centered at ~3100 cm^{-1}). UV−vis−NIR (KBr pellet; nm): λ_{max} = 690, 2900 ("A" band). EDX (at. %): Au/Ni = 78/22; M/S (metal/sulphur) = 94/6 (calcd 94/6).

[DT-TTF][Au$_{0.75}$Pt$_{0.25}$(mnt)$_2$] (3). IR (KBr pellet; cm^{-1}): ν = 3114, 1517, 1464, 1348, 1301, 1150, 1108, 903, 857, 781, 484. UV−vis−NIR (KBr pellet; nm): λ_{max} = 620. EDX (at. %): Au/Pt = 76/24; M/S = 90/10 (calcd 91/9).

[DT-TTF]$_n$[Au$_{0.55}$Pt$_{0.45}$(mnt)$_2$]$_m$ (3′). EDX (at. %): Au/Pt = 55/45; M/S = 91/9 (calcd 91/9). The M/S ratio suggests $m = n = 1$, but XRPD indicates that another polymorphic crystalline phase, different from **3**, was obtained.

[(DT-TTF)$_2$][Au$_x$Ni$_y$(mnt)$_2$] (2′). EDX (at. %): M/S = 94/6 (calcd 94/6). The detection of less than 5% content of Ni with respect to Au falls below the limit of detection of the technique. Therefore, we characterize this compound as $x > 0.95$ and $y < 0.05$.

[DT-TTF][Au$_x$Ni$_y$(mnt)$_2$] (3$_{Ni}$). EDX (at. %): M/S = 92/8 (calcd 91/9). The detection of less than 5% content of Ni with respect to Au falls below the limit of detection of the technique. Therefore, we characterize this compound as $x > 0.95$ and $y < 0.05$.

[(DT-TTF)$_2$][Au$_x$Pt$_y$(mnt)$_2$] (1$_{Au(Pt)}$). EDX (at. %): M/S = 94/6 (calcd 94/6). The detection of less than 5% content of Pt with respect to Au falls below the limit of detection of the technique. Therefore, we characterize this compound as $x > 0.95$ and $y < 0.05$. However, EPR studies confirm the presence of Pt as dopant (see text).

EDX Analysis. Crystals were placed on a graphite support and analyzed by energy dispersive X-ray microanalysis. Different parts of the crystals, for each crystalline morphologies, were analyzed to ensure the homogeneous distribution of the doping content. The

Table 2. Summarized Structural and Physical Data for the Compounds Studied

formula	stoichiometry	ladderlike struct	σ_{RT} (s cm^{-1})	S (μV K^{-1})	EPR line width at RT	ref
(DT-TTF)$_2$[(Au)(mnt)$_2$] (**1**$_{Au}$)	2:1	yes	9	38	31	6
(DT-TTF)$_2$[(Ni)(mnt)$_2$] (**1**$_{Ni}$)	2:1	yes	40	50	210	7
(DT-TTF)$_2$[(Pt)(mnt)$_2$] (**1**$_{Pt}$)	2:1	yes	40	55	600	7
(DT-TTF)$_2$[(Cu)(mnt)$_2$] (**1**$_{Cu}$)	2:1	yes	12	45	30	11
(DT-TTF)$_2$[(Au$_{0.95}$Pt$_{0.05}$)(mnt)$_2$] (**1**$_{Au(Pt)}$)	2:1	yes	13	46	123	this work
(DT-TTF)$_2$[(Au$_{0.75}$Ni$_{0.25}$)(mnt)$_2$] (**2**)	2:1	no			43	this work
(DT-TTF)$_2$[(Au$_{0.95}$Ni$_{0.05}$)(mnt)$_2$] (**2′**)	2:1	no				this work
(DT-TTF)[(Au$_{0.75}$Pt$_{0.25}$)(mnt)$_2$] (**3**)	1:1	no			200	this work
(DT-TTF)[(Au$_{0.95}$Ni$_{0.05}$)(mnt)$_2$] (**3**$_{Ni}$)	1:1	no				this work

ratios of Au metal and doping agent (Ni or Pt, respectively) were found to be reproducible within each morphology.

EPR Analysis. EPR spectra were obtained in a conventional X-band spectrometer (Bruker ESP 300 E) equipped with a microwave bridge ER041XK, a rectangular cavity operating in T102 mode, a field controller ER 032M system, and a Oxford ESR-900 cryostat, which enabled measurements in the temperature range 77−350 K. The temperature was monitored by a Au (0.07 at. % Fe)−chromel thermocouple placed close to the sample. The measurements were performed on a bulk polycrystalline sample, placed inside a quartz tube. The modulation amplitude was kept well below the line width, and the microwave power, well below saturation.

Electrical Transport Measurements. Electrical conductivity and thermoelectric power measurements were performed in the range 175−320 K in the same sample. In a first step thermopower was measured using a slow ac ($\sim 10^{-2}$ Hz) technique by attaching to the extremities along the larger dimension of the crystals with platinum paint (Demetron 308A) two i.d. = 25 μm 99.99% pure Au wires (Goodfellow Metals) anchored to two quartz thermal reservoirs, in a previously described apparatus,[16] controlled by a computer.[17] The oscillating thermal gradient was kept below 1 K, and it was measured with a differential Au−0.05 at. % Fe versus chromel thermocouple. The sample temperature was measured by a thermocouple of the same type. Both the differential thermocouple and the sample voltage were measured with Keithley 181 nanovoltmeters. The absolute thermopower of the sample was obtained after correction for the absolute thermopower of the Au leads, using the data of Huebner.[18]

In a second step, electrical resistivity measurements were performed using a four-probe technique. Without removal of the crystal from the sample holder, two extra Au wires were placed on the sample to achieve a four-in-line contact configuration. Prior to the measurements the sample was checked for unnested to nested voltage ratio, as defined by Schaeffer et al.,[19] that was below 5%. Measurements were done imposing through the sample a direct and reverse dc current in the 1 μA−10 nA range and measuring the voltage drop with a Keithley 619 electrometer.

Ab Initio XRPD Structural Analysis. The polycrystalline samples were gently ground and placed in Lindemann capillary tubes of 0.2 mm of diameter. An INEL CPS-120 Debye−Scherrer geometry diffractometer (radius = 250 mm) was used. The radiation used was Cu Kα_1 (λ = 1.540 598 Å), with a working power of 40 kV (30 mA). The detector was sensitive to a 120° position, with 4096 measure channels. The equipment contains a germanium(111) flat primary monochromator and a OSMIC Gutman Optics (no. 13B-413) reflector mirror. The beam height was 2−3 mm for all samples, and its width was 0.1 mm. Calibration was performed using $Na_2Ca_2Al_2F_{13}$ (NAC) as external reference (cubic function SPLINE). Linearization was done through PEAKOC software (from INEL). Typical measurement times were about 10 h.

Indexing of the XRPD pattern of **2** was only possible by collecting a set of high-resolution diffraction data on a well-aligned Bruker D8 Advance diffractometer (θ:θ scan), in the Bragg−Brentano mode, with the sample ground on the surface of a quartz monocrystal (zero background plate, supplied by The Gem Dugout, PA). Using TOPAS,[20] in the SVD mode, the first observed 27 peaks were indexed by a triclinic cell with a volume of 869 Å^3 (FOM = 32.4, Nc = 45). However, even if this experiment, specifically designed for indexing purposes, afforded the correct lattice metrics, the paucity and the inhomogeneity of the sample did not afford a XRPD pattern suitable for structural solution and refinement. Instead, the original data collected in capillary mode were used.

Structure solution was initiated by the simulated annealing technique implemented in TOPAS, which, in $P\bar{1}$, led to the model presented above, which contains three crystallographically independent "half" molecules, each one completed by the presence of inversion centers: at the metal for [Au$_{0.75}$Ni$_{0.25}$(mnt)$_2$] and on the middle point of the C═C vector for each of the two distinct DT-TTF moieties. In the final refinements, performed by the Rietveld method and the fundamental parameters approach, the distinct fragments were treated as rigid bodies, described by the coordinates of DT-TTF and [Au(mnt)$_2$] moieties of known literature geometry. The list of refinable parameters comprises, among others, free rotations for each rigid body, crystal size, and polynomial description of the background function. In the absence of analytical functions describing the absorption correction for cylindrical samples with $\mu R > 2.5$, an empirical polynomial function (in sin θ) was inserted as a refinable model (with B_{iso} = 4.0 or 6.0 Å^2, for the metal and the lighter atoms, respectively). Crystal data and other details of the data analysis can be found in Table 1. The final Rietveld plot is shown in Figure 11.

Indexing of **3** proved to be more difficult; indeed, TREOR90[21] suggested a number of suitable unit cells, sharing two axes (of about 24.07 and 12.28 Å) but differing in the third one, which was consistently proposed as very short (<4.1 Å). A Le Bail fit[22] with *a two-dimensional unit cell* surprisingly gave a perfect matching of the collected XRPD pattern up to $2\theta = 65°$. Thus, to detect the value (and the orientation) of the missing lattice vector, a number of further measurements were performed, in search for (not yet) indexed reflections. Once two peaks of low intensity were detected at d values of ca. 3.59 and 3.31 Å, they were assigned 111 and 131 indices, in agreement with the cell parameters proposed in Table 1. Therefore, the thin and elongated crystals, likely packed into

(16) Almeida M.; Oostra S.; Alcácer L. *Phys. Rev. B* **1984**, *30*, 2839.
(17) Lopes, E. B. Internal Report, INETI-Sacavem, 1991.
(18) Huebner, R. P. *Phys. Rev. A* **1964**, *135*, 1281.
(19) Schaffer, P. E.; Wudl, F.; Thomas, G. A.; Ferraris, J. P.; Cowan, D. O. *Solid State Commun.* **1974**, *14*, 347.
(20) Kern, A.; Coelho, A. *TOPAS*; Bruker AXS GmbH: Karlsruhe, Germany, 2003.
(21) Werner, P. E.; Eriksson, L.; Westdahl, M. *J. Appl. Crystallogr.* **1985**, *18*, 367−370.
(22) Le Bail, A.; Duroy, H.; Fourquet, J. L. *Mater. Res. Bull.* **1988**, *23*, 447−452.

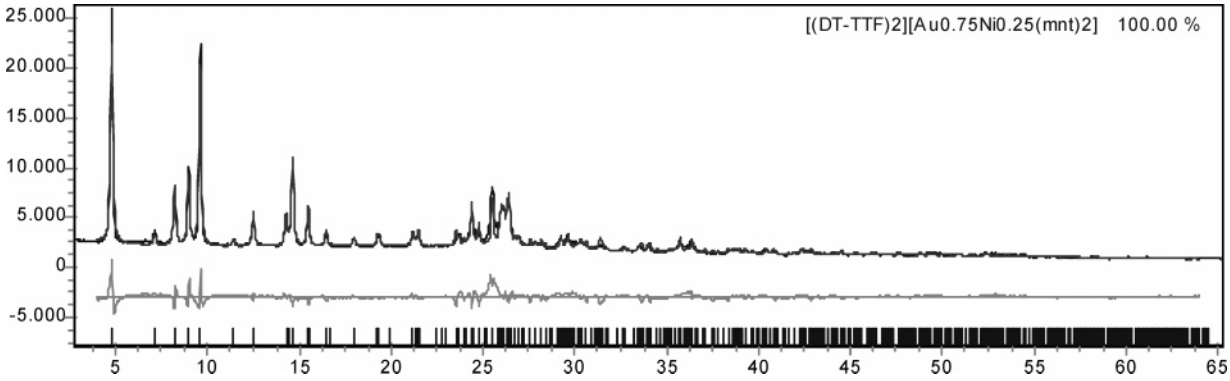

Figure 11. Final Rietveld refinement plot for (DT-TTF)$_2$[Au$_{0.75}$Ni$_{0.25}$(mnt)$_2$], **2**, with peak markers and difference plot at the bottom. The satisfactory, but still imperfect, match is attributed by the probable structural disorder of the mnt ligands, slightly displaced from their refined values, due to the presence of vicariant Ni(III) ions, of much smaller size than "host" Au(III) ions.

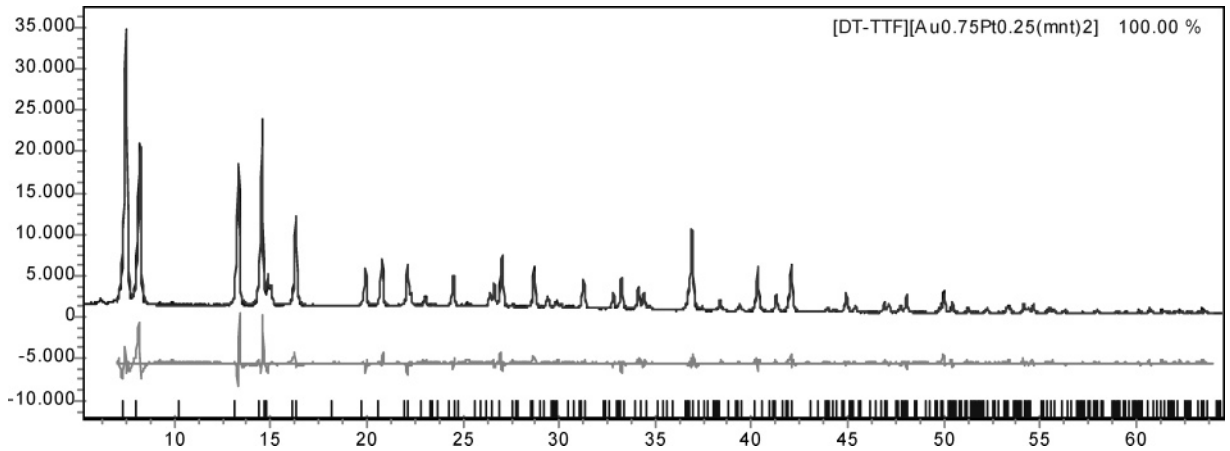

Figure 12. Final Rietveld refinement plot for (DT-TTF)[Au$_{0.75}$Pt$_{0.25}$(mnt)$_2$], **3**, with peak markers and difference plot at the bottom. Note that only peaks with $l = 0$ are present, thus forcing an unconventional refinement procedure of a 3D structural model with a nonideal XRPD pattern (i.e. with a number of missing lines).

the glass capillary as parallel bundles, have hidden, through their extreme texture effects, one axis (*c*) in the diffraction experiment. The difficulties in indexing were followed by the uncertainty of the space group. Density and geometrical considerations lead to the model presented above, of (DT-TTF)[Au$_{0.75}$Pt$_{0.25}$(mnt)$_2$] formulation. Also in this case, solution was performed by the simulated annealing technique, followed by the full Rietveld refinement in analogy with what reported above. The structure of **3** presented in this paper was eventually refined in $P2_1/a$. Note that the monoclinic angle could equally be either α or β since we have only access to one equatorial section (of $P2gg$ symmetry); we arbitrarily chose one of the two *undistinguishable* possibilities. To cope with this unconventional analysis, we forced null-intensity to reflections possessing $l \neq 0$, thus allowing the full refinement of a *three-dimensional* structural model from a diffraction pattern containing *only hk*0 reflections.[23] The correct value of the *c* parameter and of the interaxial angle β have been idealized (to 3.80 Å and 90°, respectively) and kept fixed. Crystal data and other details of the data analysis can be found in Table 1. Figure 12 shows the final Rietveld plot.

Quantitative XRPD Analysis. Once the structures of **2** and **3** were determined, the composition of polyphasic mixtures (with, or without, other crystalline contaminants) could be determined by the Rietveld method in its quantitative mode, i.e. by a whole-pattern profile refinement where only *nonstructural* parameters are set free. Scale factors are then suitably converted into relative weight proportions by simple algebraic relations.

Acknowledgment. This work was supported in Spain by the DGI Project BQU2003-00760 and by the DGR Catalonia, Project 2001SGR00362, and in Portugal by the FCT under Contract POCTI/35342/QUI/2000. The Italian MIUR and the Fondazione Provinciale Comasca are acknowledged for funding. The collaboration between authors in Barcelona and Sacavém was supported by the ICCT-CSIC bilateral agreement, and additional support was provided through COST D14.

Supporting Information Available: Complete X-ray crystallographic data for compounds **2** and **3** (CIF format). This material is available free of charge via the Internet at http://pubs.acs.org.

IC048484D

(23) A similar approach has been used in the pioneering ages of single-crystal structure determination, when, using only one or more equatorial sections of the reciprocal lattice, full three-dimensional crystal structures were retrieved.